Acta Crystallographica Section F
Structural Biology and Crystallization Communications
ISSN 1744-3091

Towards the crystal structure elucidation of eukaryotic UDP-galactopyranose mutase

Karin E. van Straaten,[a] Francoise H. Routier[b] and David A. R. Sanders[a]*

[a]Department of Chemistry, University of Saskatchewan, 110 Science Place, Saskatoon, Saskatchewan S7N 5C9, Canada, and [b]Medizinische Hochschule Hannover, Carl-Neuberg-Strasse 1, 30625 Hannover, Germany

Correspondence e-mail: david.sanders@usask.ca

Received 10 November 2011
Accepted 15 February 2012

UDP-galactopyranose mutase (UGM) catalyzes the interconversion of UDP-galactopyranose and UDP-galactofuranose. Eukaryotic UGMs from *Aspergillus fumigatus* and *Leishmania major* have been purified to homogeneity by means of Ni^{2+}-affinity chromatography and crystallized. Eukaryotic UGM structure elucidation was not straightforward owing to high pseudo-symmetry, twinning and very low anomalous signal. Phasing to 2.8 Å resolution using SAD was successful for *L. major* UGM. However, the maps could only be improved by iterative density modification and manual model building. High pseudo-symmetry and twinning prevented correct space-group assignment and the completion of structure refinement. The structure of *A. fumigatus* UGM to 2.52 Å resolution was determined by molecular replacement using the incomplete 2.8 Å resolution *L. major* UGM model.

1. Introduction

Drug-resistant pathogens cause serious health problems, creating an urgent need for alternative antibiotics and antibiotic drug targets. One such target is UDP-galactopyranose mutase (UGM). UGM catalyzes the interconversion of UDP-galactopyranose (UDP-Gal*p*) to UDP-galactofuranose (UDP-Gal*f*), a precursor for the construction of Gal*f*-containing oligosaccharides. Gal*f* is an essential component of the cell wall in bacteria and fungi and the cell-surface matrix of protozoan parasites, and appears to be essential for survival and virulence (Nassau *et al.*, 1996; Köplin *et al.*, 1997; Bernard & Latgé, 2001; de Lederkremer & Colli, 1995; Tefsen *et al.*, 2011). Since Gal*f* and UGM are not found in humans, UGM is an interesting target for novel structure-based drug design (Pedersen & Turco, 2003; Tefsen *et al.*, 2011). In order to design such drugs, detailed structural information is required.

To date, structural research on UGM has resulted in the crystal structures of four prokaryotic UGMs: those from *Escherichia coli*, *Mycobacterium tuberculosis*, *Klebsiella pneumoniae* and *Deinococcus radiodurans* (Beis *et al.*, 2005; Sanders *et al.*, 2001; Partha *et al.*, 2009). Structures of prokaryotic UGMs with and without bound substrate have been reported (Partha *et al.*, 2009; Gruber, Westler *et al.*, 2009; Gruber, Borrok *et al.*, 2009). These structures revealed the overall fold of UGM, which consists of three domains (an FAD-binding domain containing the $\alpha\beta\alpha$ Rossmann fold, an α-helix domain and a β-sheet domain), and shed light on how substrate is bound in prokaryotic UGMs. In addition, examination of these structures confirmed that the active site of UGM closes around the substrate as it binds and is controlled by an invariant arginine residue that interacts with the diphosphate of the substrate (Partha *et al.*, 2009; Gruber, Westler *et al.*, 2009). Eukaryotic UGMs are less well characterized, but have been identified and characterized in several eukaryotic organisms such as *Aspergillus fumigatus*, *A. niger*, *A. nidulans*, *Leishmania major* and *Trypanosoma cruzi* (Beverley *et al.*, 2005; Bakker *et al.*, 2005; Kleczka *et al.*, 2004; Oppenheimer *et al.*, 2010, 2011; El-Ganiny *et al.*, 2008). Eukaryotic UGMs share less than 30% identity to bacterial UGMs, but most residues required for substrate and FAD binding are conserved (Chad *et al.*, 2007; Beverley *et al.*,

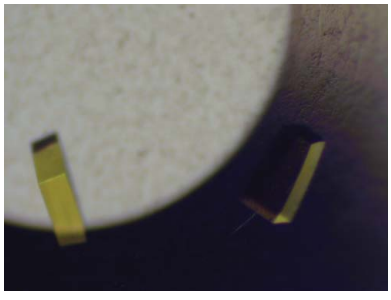

2005). Eukaryotic UGMs have additional inserts in their sequence compared with prokaryotic UGMs, although the role of these additional inserts is not yet known. Furthermore, while prokaryotic UGMs are dimers, *A. fumigatus* UGM (AfUGM) has been reported to function as a tetramer (Oppenheimer *et al.*, 2010) and *L. major* UGM (LmUGM) as a monomer (Oppenheimer *et al.*, 2011).

Our laboratory is currently focusing on determining the structures of the UGMs from the eukaryotic pathogens *A. fumigatus* (AfUGM) and *L. major* (LmUGM). UGM gene deletions in *A. fumigatus* and *L. major* lead to attenuated virulence, decreased cell-wall thickness and increased sensitivity to antifungal agents (Schmalhorst *et al.*, 2008; Kleczka *et al.*, 2004). To increase our knowledge of molecular details and mechanisms, we aim to determine the crystal structures of eukaryotic UGMs and to compare their structures with those of prokaryotic UGMs.

This paper describes the purification, crystallization and unusual structure determination of eukaryotic UGMs from *A. fumigatus* and *L. major*.

2. Materials and methods

2.1. Expression and purification of native LmUGM

A pET22b plasmid containing the *LmUGM* gene (AJ871146) with a C-terminal His tag (*E. coli* clone 1666) was used for overexpression of *L. major* UGM (LmUGM; Kleczka *et al.*, 2004). Briefly, *E. coli* strain BL21 (DE3) Gold was used to express LmUGM. The cells were cultured at 303 K and 250 rev min^{-1} in LB medium containing 50 µg ml^{-1} ampicillin. The cells were allowed to grow to an OD_{600} of 0.5. The culture was shifted to 288 K and allowed to grow for 30 min. Expression was induced by addition of 0.5 m*M* IPTG and the culture was grown for a further 24 h. The cells were harvested, resuspended in PBS buffer pH 7.3 (2.7 m*M* KCl, 137 m*M* NaCl, 8.1 m*M* Na_2HPO_4, 1.76 m*M* KH_2PO_4) and incubated with 20 mg ml^{-1} lysozyme and 20 U ml^{-1} DNase for 1 h while stirring at 277 K. After incubation, the cells were ruptured by sonication and cell debris was removed by centrifugation at 15 000 rev min^{-1} for 30 min. The pellets were resuspended in PBS buffer pH 7.3 containing 0.5 m*M* tris(2-carboxyethyl)phosphine–HCl (TCEP) and 0.2% sodium deoxycholate, briefly sonicated and centrifuged. The pooled supernatants were loaded onto a Protino Ni-IDA binding column (Macherey-Nagel). His_6-tagged LmUGM was eluted with 250 m*M* imidazole in PBS buffer pH 7.3. Fractions were analyzed by SDS–PAGE. Fractions containing pure His_6-tagged LmUGM were pooled and dialyzed overnight against 20 m*M* Tris pH 8.0 with 1 m*M* TCEP. His_6-tagged LmUGM was concentrated to 14 mg ml^{-1} using a 30K Amicon centrifugal filter device. Protein concentration was determined using UV-absorption spectroscopy at 280 nm with a theoretical molecular extinction coefficient of 1.789. Around 60 mg pure protein was obtained from a 4 l LB culture. The recombinant protein contained eight non-native residues (LEHHHHHH) at the C-terminus.

2.2. Expression and purification of native AfUGM

A pET22b plasmid containing the *AfUGM* gene (AJ871145) with a C-terminal His tag (*E. coli* clone 2212) was used for overexpression of AfUGM (Schmalhorst *et al.*, 2008). Briefly, *E. coli* strain BL21 (DE3) Gold (Novagen) was used to express AfUGM. Cells harbouring pET22b expression vector for overexpression of C-terminally His_6-tagged AfUGM were cultured at 303 K and 250 rev min^{-1} in LB medium containing 50 µg ml^{-1} ampicillin. Expression was induced by the addition of 1 m*M* IPTG when the cell density reached an optical density (OD_{600}) of 0.6–0.8. Cells were grown for an additional 4 h, harvested and resuspended in lysis buffer (buffer *A*) containing 5 m*M* imidazole, 0.50 *M* NaCl, 0.1% NaN_3, 50 m*M* bis-tris-propane pH 7.7. After the addition of 2 m*M* lysozyme, 1 m*M* AEBSF and 20 µg l^{-1} DNAse, the cells were ruptured by sonication and cell debris was removed by centrifugation at 8000 rev min^{-1} for 30 min at 277 K. Ammonium sulfate precipitation (10% ammonium sulfate) was carried out on the supernatant containing AfUGM. The supernatant was clarified by centrifugation at 17 000 rev min^{-1} for 30 min at 277 K. The supernatant was filtered through 0.22 µm filters and loaded onto a 10 ml Ni-loaded chelating column (MC20, Applied Biosystems) pre-equilibrated with buffer *A* at 295 K. The column was washed with seven column volumes of buffer *A*. Bound His_6-tagged AfUGM was eluted with a linear imidazole gradient from 5 to 600 m*M* imidazole in 50 m*M* bis-tris-propane pH 7.7 containing 0.5 *M* NaCl at a flow rate of 10 ml min^{-1}. His_6-tagged AfUGM eluted at about 100 m*M* imidazole. Fractions were analyzed by SDS–PAGE. Fractions containing His_6-tagged AfUGM (molecular weight 58 kDa) were pooled and dialyzed against 25 m*M* Tris–malonate pH 8.0. His_6-tagged AfUGM was concentrated to 24.6 mg ml^{-1} using a 30K Amicon centrifugal filter device. The amount of protein was determined using UV-absorption spectroscopy at 280 nm with a theoretical molecular extinction coefficient of 1.608. Around 73 mg pure protein was obtained from a 4 l LB culture. The recombinant protein contained eight non-native residues (LEHHHHHH) at the C-terminus.

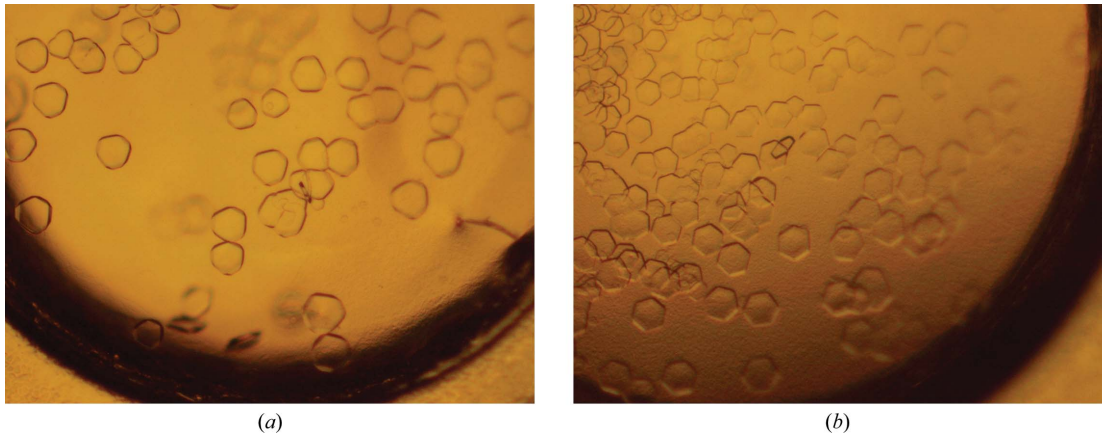

(*a*) (*b*)

Figure 1
Trigonal (*a*) and hexagonal (*b*) crystals of LmUGM.

2.3. Expression and purification of SeMet-AfUGM and SeMet-LmUGM

Selenomethionine-substituted AfUGM (SeMet-AfUGM) and LmUGM (SeMet-LmUGM) were prepared using *E. coli* cells grown in 2× M9 minimal medium and supplemented 15 min before induction with 46 mg l^{-1} L-selenomethionine and a mixture of amino acids known to inhibit methionine biosynthesis (Doublié, 1997; Gerchman *et al.*, 1994). Purification of SeMet-substituted enzymes was carried out as described above but with 5 m*M* TCEP included in the buffers to prevent the oxidation of selenomethionine. 140 mg pure SeMet-AfUGM was obtained from a 4 l M9-SeMet high-yield growth culture (Medicillon Inc.). SeMet-AfUGM was concentrated to 12.0 mg ml^{-1} in 25 m*M* Tris–malonate pH 8.0, 5 m*M* TCEP. About 87 mg pure SeMet-LmUGM was obtained from a 4 l M9-SeMet high-yield growth culture (Medicillon Inc.). SeMet-LmUGM was concentrated to 26.0 mg ml^{-1} in 25 m*M* Tris–malonate pH 8.0, 1 m*M* TCEP.

2.4. Crystallization of LmUGM

Initial crystal screening for LmUGM was conducted using the microbatch method at 277 K. Initial screening for crystallization conditions was performed using commonly available commercial screens from Qiagen. The microbatch drops were prepared by mixing equal volumes of protein solution (1.2 µl; 22.0 mg ml^{-1} LmUGM in 25 m*M* Tris pH 8.0) and precipitant solution (1.2 µl). The crystallization drop was overlaid with paraffin oil to prevent the evaporation of water from the drop. Plate-like crystals of LmUGM were grown in 20–40% PEG 3350. The best crystals were obtained using the hanging-drop vapour-diffusion method and using a higher LmUGM concentration. Hanging drops were prepared by mixing equal volumes of protein solution (1.2 µl; 34.0 mg ml^{-1} LmUGM in 25 m*M* Tris pH 8.0) and well solution (1.2 µl) and were equilibrated against 500 µl well solution. Hexagonal and trigonal plate-shaped crystals (Fig. 1) were obtained in 10–20% PEG 3350 and 0–15% 2-propanol. The crystals appeared within a week after setup. SeMet-LmUGM crystallized under the same crystal conditions as native LmUGM.

2.5. Crystallization of AfUGM

Crystals of AfUGM were grown at both 277 and 293 K using the sitting-drop vapour-diffusion method and using a modified microbatch method that uses a 50:50 mixture of silicone oil and paraffin oil (Al's oil) to cover the drops (D'Arcy *et al.*, 1996, 2004). Initial screening for crystallization conditions was performed using commonly available commercial screens from Qiagen. The microbatch drops were prepared by mixing equal volumes of protein solution (1.2 µl; 10.3 mg ml^{-1} AfUGM, 20 m*M* UDP-Gal*p* in 25 m*M* Tris pH 8.0) and precipitant solution (1.2 µl). The crystallization drop was overlaid with Al's oil, allowing the slow evaporation of water from the drop. Crystals of AfUGM were found in several different conditions. Three crystal forms of AfUGM were found (tetragonal-shaped, plate-shaped and rod-shaped crystals). Tetragonal crystals (crystal form I) were obtained using the hanging-drop method at 277 K. Briefly, hanging drops were prepared by mixing equal volumes of protein solution (1.2 µl; 10.3 mg ml^{-1} AfUGM, 20 m*M* UDP-Gal*p* in 25 m*M* Tris pH 8.0) and well solution (1.2 µl) and were equilibrated against 1 ml well solution (0.1 *M* sodium acetate pH 4.2, 1.53 *M* ammonium sulfate). The best plate-shaped (crystal form II) and rod-shaped (crystal form III) crystals grew both at 277 and 293 K (Fig. 2). The plate-shaped and rod-shaped crystals were obtained using the microbath method in 0.1–0.2 *M* salt ($NaNO_2$ or sodium citrate), 10–25% PEG 3350 and 0.1 *M* bis-tris (propane) buffer pH 5.5–8.5. SeMet-AfUGM crystallized under the same crystal conditions as native AfUGM. All crystal forms appeared within a week after setup.

2.6. Data collection and processing

Crystals were flash-cooled in mother liquor containing 20%(*v*/*v*) ethylene glycol as a cryoprotectant. X-ray diffraction intensity data were collected on beamline 08ID-1 at the CLS using a MAR 225 CCD detector.

A high-redundancy SAD data set was collected from a single SeMet-LmUGM crystal at the CLS using a MAR 225 CCD detector. A total of 720 frames were collected with 0.5° oscillation and 0.5 s exposure time per image; the crystal-to-detector distance was 200 mm.

A total of 800 frames were collected from AfUGM crystal form I with 0.25° oscillation and 10 s exposure time per image; the crystal-to-detector distance was 200 mm. A total of 400 frames were collected from AfUGM crystal form II and AfUGM crystal form III with 0.5° oscillation and 1 s exposure time per image. The wavelength was 0.9795 Å and the crystal-to-detector distances were 210 and 190 mm, respectively. Prior to MAD data collection, an Se absorption-edge scan was collected to determine the peak, inflection-point and remote wavelengths. MAD data were collected from an SeMet-AfUGM crystal (form I) at three wavelengths around the Se *K* edge: 0.9793 Å (peak), 0.9794 Å (inflection point) and 0.97467 Å (remote). A total of 360 frames per wavelength were collected with 0.5° oscillation and 2 s exposure time per image; the crystal-to-detector distance was 450 mm.

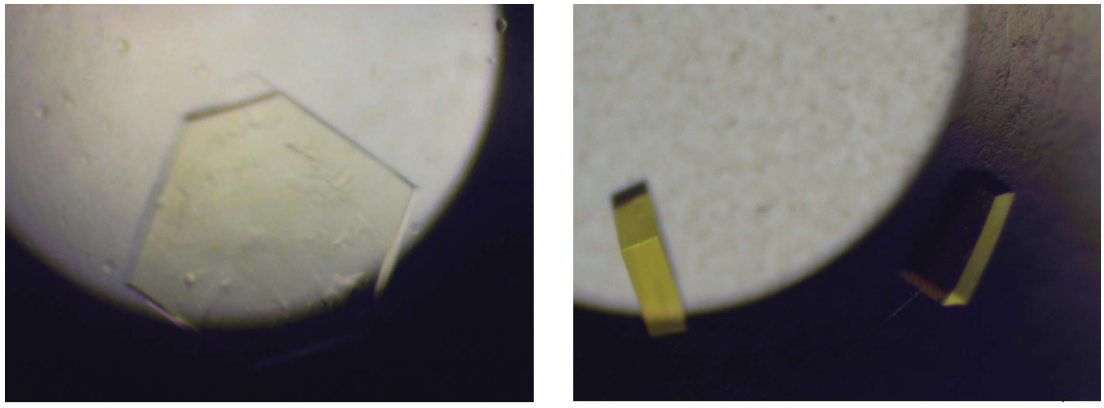

(*a*) (*b*)

Figure 2
Crystal form II (*a*) and crystal form III (*b*) of AfUGM.

Table 1
Data-collection statistics for AfUGM and LmUGM and phasing statistics for LmUGM.

Values in parentheses are for the highest resolution shell.

	SeMet-AfUGM form I	AfUGM form II	AfUGM form III	SeMet-LmUGM
Beamline	08ID-1, CLS	08ID-1, CLS	08ID-1, CLS	08ID-1, CLS
Wavelength (Å)	0.9793 [peak], 0.9794 [inflection], 0.97467 [remote]	0.9795	0.9795	0.9793 [peak]
Space group	$P4_122/P4_322$	$P2_1$	$P1$	$P3_121$
Unit-cell parameters (Å)	$a = b = 213.1$, $c = 420.7$, $\alpha = \beta = \gamma = 90.0$	$a = 72.7$, $b = 125.7$, $c = 156.0$, $\alpha = \gamma = 90$, $\beta = 101$	$a = 71.7$, $b = 129.0$, $c = 173.5$, $\alpha = 89.8$, $\beta = 84.6$, $\gamma = 81.1$	$a = b = 82.0$, $c = 134.6$, $\alpha = \beta = 90$, $\gamma = 120$
Resolution (Å)	40.0–2.75 (2.85–2.75)	19.8–3.00 (3.10–3.00)	19.9–2.52 (2.57–2.52)	50.0–2.80 (2.90–2.80)
Measured reflections	2213093	177567	421458	265829
Unique reflections	249476	47710	194408	13569
Completeness (%)	100.0 (100.0)	95.1 (66.5)	94.4 (90.2)	99.9 (100.0)
$\langle I/\sigma(I)\rangle$	7.5 (1.9)	17.5 (9.1)	11.5 (3.4)	58.7 (4.9)
R_{merge} (%)	17.7 (61.8)	5.9 (12.1)	5.2 (24.2)	9.7 (82.4)
Monomers per asymmetric unit	16	4	8	1
Phasing statistics				
Se sites (found/all)				22
FOM				0.36
FOM after density modification				0.58

All native diffraction data were indexed and integrated using *XDS* (Kabsch, 2010) and scaled and merged using *XSCALE* and *XDSCONV*. The anomalous diffraction data were processed and scaled using *HKL*-2000 (Otwinowski & Minor, 1997). The unit-cell parameters and space-group information and the statistics for the best data set collected from each crystal form are given in Table 1.

3. Results and discussion

3.1. Crystallization and data collection for LmUGM

Hexagonal-shaped and trigonal-shaped plate-like crystals of LmUGM were obtained using the hanging-drop vapour-diffusion method. LmUGM crystallized in space group $P3_121$ with only one molecule in the asymmetric unit. These crystals diffracted to a maximum of 2.5 Å resolution at the synchrotron. Examination of the diffraction pattern showed strong diffraction interspersed with a weaker diffracting lattice, suggesting either pseudo-translation and/or twinning (Fig. 3). However, processing and scaling in a larger cell was not possible. Furthermore, a self-rotation function in $P1$ at 2.8 Å was inconclusive.

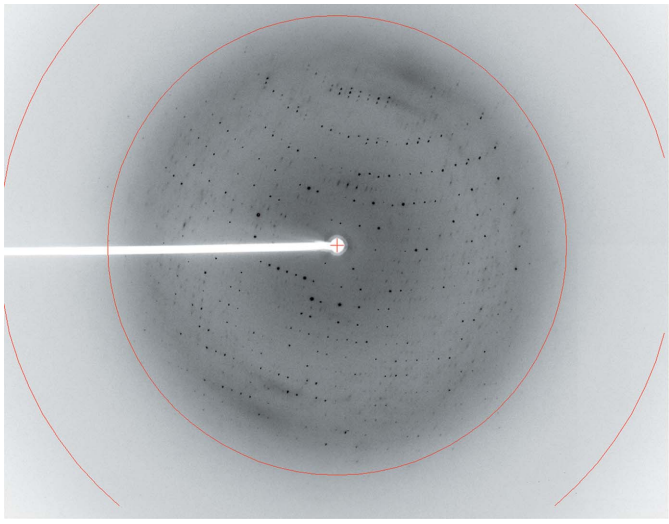

Figure 3
Diffraction pattern of LmUGM showing two lattices.

3.2. Experimental phasing, model building and refinement for LmUGM

The crystal structure of LmUGM was determined in space group $P3_121$ to 2.8 Å resolution using selenomethionine single-wavelength anomalous dispersion (SAD). Phase calculation, density modification and preliminary model building were carried out using *PHENIX AutoSol* and *AutoBuild* (Adams *et al.*, 2010). *PHENIX AutoSol* found 22 selenium sites; 13 of these were expected and nine were either the result of alternate configurations of the SeMet residues or a consequence of twinning. The initial electron-density maps after density modification in *PHENIX* showed clear density for the β-sheet domain. The electron density for the α-helix and FAD domains was of poor quality, only showing density for a few α-helices and β-strands. *Buccaneer* (Cowtan, 2006) was able to build part of the amino-acid residues for the β-sheet and FAD domains. Manual model rebuilding was performed in *Coot* (Emsley & Cowtan, 2004) using the 13 SeMet positions and the crystal structures of protoporphyrinogen oxidase (PPOX) from *Bacillus subtilis* (PDB entry 3i6d; Qin *et al.*, 2009) and prokaryotic UGM from *K. pneumoniae* (PDB entry 3gf4; Gruber, Borrok *et al.*, 2009) as guides. Refinement (rigid-body refinement and simulated annealing starting at 5000 K) of the LmUGM model against experimental data in *PHENIX* in space group $P3_121$ resulted in high R factors (R = 45%, R_{free} = 50%). Experimental phases and electron-density maps were improved by density modification in *OASIS* (He *et al.*, 2007) using the partially built model, 13 SeMet positions and the experimental data. Iterative manual model building in *Coot* and phase improvement using density modification in *OASIS* resulted in a model with 75% of the amino acids being built into electron density. The refinement still stalled at high R factors (R = 36.3% and R_{free} = 48.7%) and no further map improvements were apparent. Data were reprocessed in *HKL*-2000 in space groups $P3_1$ and $C2$. Space group $P3_1$ showed no improvement compared with $P3_121$ and was not considered. A possible explanation is that this is not the correct space group owing to high pseudo-symmetry, although tests were unclear. We therefore reprocessed our data in the lower symmetry space group $C2$. Molecular replacement in $C2$ using the $P3_121$ LmUGM model gave a clear solution. The rotation search gave three top solutions with an Rf/σ values of 9.6, 9.4 and 8.9 (in contrast to 3.5 for the fourth solution), which suggested the presence of three monomers per asymmetric unit. The best solution after the translation function had an R factor of 48.2%. Rigid-body refinement and simulated annealing starting at 5000 K using NCS gave an R factor of

32.4% and an R_{free} of 37.8%. *phenix.xtriage* indicated near-perfect twinning with the following two twin operators: $0.5h + 1.5k$, $0.5h - 0.5k$, $-l$ and $0.5h + 1.5k$, $-0.5h - 0.5k$, $-l$. The same drop in R factors (R = 32.2% and R_{free} = 36.5%) was observed when either of the twin operators was applied. Furthermore, $2F_o - F_c$ and $F_o - F_c$ electron-density maps showed additional density for main chains and side chains. Manually rebuilding part of the structure in *Coot* and subsequent refinement in *PHENIX* (simulated annealing at 2500 K and applying NCS using twin operator $0.5h + 1.5k$, $0.5h - 0.5k$, $-l$) lowered the R factors (R = 30.5% and R_{free} = 35.5%). Currently, we are in the process of overcoming the twinning and completing our refinement of the LmUGM model.

3.3. Molecular replacement and experimental phasing trials for AfUGM

Native and SeMet-substituted AfUGM have been expressed and purified to homogeneity. Diffraction-quality crystals have been grown in three different crystal forms and the crystal parameters and data-collection statistics are summarized in Table 1. The best diffracting crystal (crystal form III) diffracted to about 2.3 Å resolution. On the basis of density calculations and the fact that the protein is a tetramer in solution (Oppenheimer *et al.*, 2010), we estimate that eight molecules of the protein are present per asymmetric unit (V_M = 3.38 Å^3 Da^{-1}, solvent content 64.5%; Matthews, 1968). On the basis of density calculations (V_M = 2.92 Å^3 Da^{-1}, solvent content 57.9%), we estimate that crystal form II would only contain one tetramer. For crystal form I, we expect four tetramers per asymmetric unit (V_M = 2.55 Å^3 Da^{-1}, solvent content 51.8%), although other arrangements also fall within reasonable Matthews values. Although the crystal structures of prokaryotic UGMs were available, our initial attempts to solve the AfUGM structure by molecular replacement using *MOLREP* (Vagin & Teplyakov, 2010), *Phaser* (McCoy *et al.*, 2007) or *MrBUMP* (Keegan & Winn, 2007) failed. All molecular-replacement trials using either the whole or the three separate domains (FAD, β-sheet and α-helix domains) of known prokaryotic UGM structures from *E. coli* (PDB entry 1i8t; Sanders *et al.*, 2001), *M. tuberculosis* (PDB entry 1v0j; Beis *et al.*, 2005) and *K. pneumonia* (PDB entries 1wam, 2bi7 and 2bi8; Beis *et al.*, 2005) as search models failed to give a good solution.

Several MAD and SAD data sets were collected from all three crystal forms of SeMet-substituted AfUGM. Radiation sensitivity or a too weak anomalous signal prevented the determination of the substructure of AfUGM.

3.4. Structure determination of AfUGM

The model of SeMet-LmUGM was used to determine the phases for the AfUGM data sets. AfUGM shares 46% sequence identity with LmUGM. Initial phases for the AfUGM data were obtained by molecular replacement with *MrBUMP* (Keegan & Winn, 2007) using *MOLREP* (Vagin & Teplyakov, 2010) and the LmUGM structure. All three crystal forms of AfUGM were used for molecular replacement, but crystal form III gave the best results. Molecular replacement in *P*1 using the LmUGM model gave a solution (R = 54.4%, score = 0.583). Initial rigid-body refinement and simulated annealing starting at 5000 K using NCS gave an R factor of 38.7% and an R_{free} of 42.1%. Inspection of the model in *Coot* showed no clashes. The solution has two tetramers per asymmetric unit. The initial $F_o - F_c$ electron-density map showed clear density for FAD. Further refinement and additional model building are currently in progress, for which structural details will be described in a separate paper. In addition, we intend to perform X-ray crystallographic studies of AfUGM with substrate and inhibitors to determine cocrystal structures.

We would like to thank the staff of macromolecular beamline 08ID-1, Canadian Light Source (CLS), Saskatoon, Saskatchewan, Canada for their technical assistance during data collection. The research described in this paper was performed at the CLS, which is supported by NSERC, the National Research Council of Canada, the Canadian Institutes of Health Research, the Province of Saskatchewan, Western Economic Diversification Canada and the University of Saskatchewan. This work was supported by a CIHR-RPP grant and an NSERC grant to DARS and an SHRF-PDF to KVS.

References

Adams, P. D. *et al.* (2010). *Acta Cryst.* D**66**, 213–221.
Bakker, H., Kleczka, B., Gerardy-Schahn, R. & Routier, F. H. (2005). *Biol. Chem.* **386**, 657–661.
Beis, K., Srikannathasan, V., Liu, H., Fullerton, S. W., Bamford, V. A., Sanders, D. A., Whitfield, C., McNeil, M. R. & Naismith, J. H. (2005). *J. Mol. Biol.* **348**, 971–982.
Bernard, M. & Latgé, J. P. (2001). *Med. Mycol.* **39**, Suppl. 1, 9–17.
Beverley, S. M., Owens, K. L., Showalter, M., Griffith, C. L., Doering, T. L., Jones, V. C. & McNeil, M. R. (2005). *Eukaryot. Cell*, **4**, 1147–1154.
Chad, J. M., Sarathy, K. P., Gruber, T. D., Addala, E., Kiessling, L. L. & Sanders, D. A. (2007). *Biochemistry*, **46**, 6723–6732.
Cowtan, K. (2006). *Acta Cryst.* D**62**, 1002–1011.
D'Arcy, A., Elmore, C., Stihle, M. & Johnston, J. E. (1996). *J. Cryst. Growth*, **168**, 175–180.
D'Arcy, A., Sweeney, A. M. & Haber, A. (2004). *Methods*, **34**, 323–328.
Doublié, S. (1997). *Methods Enzymol.* **276**, 523–530.
El-Ganiny, A. M., Sanders, D. A. & Kaminskyj, S. G. (2008). *Fungal Genet. Biol.* **45**, 1533–1542.
Emsley, P. & Cowtan, K. (2004). *Acta Cryst.* D**60**, 2126–2132.
Gerchman, S. E., Graziano, V. & Ramakrishnan, V. (1994). *Protein Expr. Purif.* **5**, 242–251.
Gruber, T. D., Borrok, M. J., Westler, W. M., Forest, K. T. & Kiessling, L. L. (2009). *J. Mol. Biol.* **391**, 327–340.
Gruber, T. D., Westler, W. M., Kiessling, L. L. & Forest, K. T. (2009). *Biochemistry*, **48**, 9171–9173.
He, Y., Yao, D.-Q., Gu, Y.-X., Lin, Z.-J., Zheng, C.-D. & Fan, H.-F. (2007). *Acta Cryst.* D**63**, 793–799.
Kabsch, W. (2010). *Acta Cryst.* D**66**, 125–132.
Keegan, R. M. & Winn, M. D. (2007). *Acta Cryst.* D**63**, 447–457.
Kleczka, B., Lamerz, A. C., Bakker, H., Wiese, M., Gerardy-Schahn, R. & Routier, F. H. (2004). *Glycobiology*, **14**, 1119.
Köplin, R., Brisson, J. R. & Whitfield, C. (1997). *J. Biol. Chem.* **272**, 4121–4128.
Lederkremer, R. M. de & Colli, W. (1995). *Glycobiology*, **5**, 547–552.
Matthews, B. W. (1968). *J. Mol. Biol.* **33**, 491–497.
McCoy, A. J., Grosse-Kunstleve, R. W., Adams, P. D., Winn, M. D., Storoni, L. C. & Read, R. J. (2007). *J. Appl. Cryst.* **40**, 658–674.
Nassau, P. M., Martin, S. L., Brown, R. E., Weston, A., Monsey, D., McNeil, M. R. & Duncan, K. (1996). *J. Bacteriol.* **178**, 1047–1052.
Oppenheimer, M., Poulin, M. B., Lowary, T. L., Helm, R. F. & Sobrado, P. (2010). *Arch. Biochem. Biophys.* **502**, 31–38.
Oppenheimer, M., Valenciano, A. L. & Sobrado, P. (2011). *Biochem. Biophys. Res. Commun.* **407**, 552–556.
Otwinowski, Z. & Minor, W. (1997). *Methods Enzymol.* **276**, 307–326.
Partha, S. K., van Straaten, K. E. & Sanders, D. A. (2009). *J. Mol. Biol.* **394**, 864–877.
Pedersen, L. L. & Turco, S. J. (2003). *Cell. Mol. Life Sci.* **60**, 259–266.
Qin, X., Sun, L., Wen, X., Yang, X., Tan, Y., Jin, H., Cao, Q., Zhou, W., Xi, Z. & Shen, Y. (2009). *J. Struct. Biol.* **170**, 76–82.
Sanders, D. A., Staines, A. G., McMahon, S. A., McNeil, M. R., Whitfield, C. & Naismith, J. H. (2001). *Nature Struct. Biol.* **8**, 858–863.
Schmalhorst, P. S., Krappmann, S., Vervecken, W., Rohde, M., Müller, M., Braus, G. H., Contreras, R., Braun, A., Bakker, H. & Routier, F. H. (2008). *Eukaryot. Cell*, **7**, 1268–1277.
Tefsen, B., Ram, A. F. J., Van Die, I. & Routier, F. H. (2011). *Glycobiology*, **22**, 456–469.
Vagin, A. & Teplyakov, A. (2010). *Acta Cryst.* D**66**, 22–25.